HOKKAIDO UNIVERSITY

Title	Enhanced upwelling in the eastern equatorial Pacific at the last five glacial terminations
Author(s)	bin Shaari, Hasrizal; Yamamoto, Masanobu; Irino, Tomohisa
Citation	Palaeogeography palaeoclimatology palaeoecology, 386, 8-15 https://doi.org/10.1016/j.palaeo.2013.03.022
Issue Date	2013-09-15
Doc URL	https://hdl.handle.net/2115/53618
Rights	Copyright © 2013 Elsevier B.V. All rights reserved.
Type	journal article
File Information	Shaari_Palaeo2013.pdf

Hokkaido University Collection of Scholarly and Academic Papers : HUSCAP

Enhanced upwelling in the eastern equatorial Pacific at the last five glacial terminations

Hasrizal bin Shaari*, Masanobu Yamamoto and Tomohisa Irino

Faculty of Environmental Earth Science, Hokkaido University,
Kita-10, Nishi-5, Kita-ku, Sapporo 060-0810, Japan.

*Corresponding author: Tel.:+81-11-706-2379, fax:+81-11-706-4867
E-mail address: hasrizals@ees.hokudai.ac.jp (S.Hasrizal)

Keywords: TEX_{86}, U^{K}_{37}', eastern equatorial Pacific, upwelling, deglaciation

Abstract

TEX_{86}^{H}- and U^{K}_{37}'-derived paleotemperatures, and isoprenoid glycerol dialkyl glycerol tetraether (GDGT), and alkenone concentrations were examined for ODP Site 1239 in the eastern equatorial Pacific (EEP) for the last 430 kyrs. We propose that the difference between TEX_{86}^{H}- and U^{K}_{37}'-derived temperatures (ΔT) and the abundance ratio of GDGTs to alkenones (GDGT/alkenone ratio) are potential upwelling indices which show a consistent results with other upwelling indices. The ΔT and GDGT/alkenone ratio were maximal during the last five deglaciations, suggesting intensified upwelling. The intensification of upwelling in the EEP coincided with those at the Peru margin and in the Southern Ocean. This coincidence suggests that the reorganization of the Southern

Hemisphere atmospheric circulation induced the intensification of the subtropical high-pressure cell, causing stronger southeast trade winds along the west coast of South America and the southern westerlies over the Southern Ocean, enhancing upwelling in both regions.

1. Introduction

The eastern equatorial Pacific (EEP) is a region between subtropical gyres of the North and South Pacific and contains the eastern terminus of the equatorial current system of the Pacific (Kessler et al., 2006). This region is important for its roles in climate variability as a result of the El Niño-Southern Oscillation (ENSO) and its significance for global carbon cycle (Fiedler and Lavin, 2006).

Glacial-interglacial changes in the oceanic condition of the EEP have been reconstructed by various studies, including of sea surface temperature (SST) (e.g., Lyle et al., 1992), salinity (e.g., Lea et al., 2000), export production (e.g., Lyle et al., 1988), and intermediate water properties (e.g., Spero and Lea, 2002; Ganeshram et al., 2000). These studies have provided evidence for an early response by the EEP to orbital forcing (e.g., Imbrie et al., 1992), and the EEP is thus thought to play an important role in amplifying climatic changes through positive feedback mechanisms.

ENSO-like variability has often been used to interpret changes in the oceanic condition of the EEP (e.g., Lea et al., 2000; Koutavas et al., 2002), but different proxy records have led to different conclusions. Some researchers, for instance, have suggested that the glacial EEP was El Niño-like based on foraminiferal Mg/Ca and $\delta^{18}O$ (e.g., Koutavas et al., 2002; Koutavas and Lynch-Stieglitz, 2003), but others have inferred a

glacial La Niña-like condition (e.g., coccolith assemblages by Beaufort et al., 2001; foraminiferal assemblages by Martinez et al., 2003; alkenones by Rincon-Martinez et al., 2010). This disagreement has been attributed to differences in the behavior of different proxies (e.g., Dubois et al., 2009).

In this paper, we present temperature records derived from TEX_{86}^{H} and U^{K}_{37}' for Ocean Drilling Program (ODP) Site 1239 and interpret the U^{K}_{37}' and TEX_{86}^{H} records for the last 430,000 years. On the basis of this interpretation, we propose the difference between TEX_{86}^{H}- and U^{K}_{37}'-derived temperatures and the abundance ratio of glycerol dialkyl glycerol tetraethers (GDGTs) to alkenones as potential upwelling indices and discuss the response of the EEP upwelling system to orbital forcing.

Modern physical oceanography

The zonal surface current system in the eastern tropical Pacific (ETP) consists of westward- and eastward-flowing currents (Fig. 1). The main westward currents are the North Equatorial Current (NEC; 8°N and 20°N) and the South Equatorial Current (SEC; 3°N to 10°S). The SEC originates as a combination of the waters from the North Equatorial Counter Current (NECC), the Equatorial Undercurrent (EUC), and the Peruvian Undercurrent (Kessler, 2006) through equatorial upwelling, mixing and advection. Two main lobes of the SEC are observed at latitude of about 3°S to just north of the equator. The NECC, an eastward current flows just north of the equator and is centered at about 5°N (Wyrtki, 1967; Talley et al., 2011). This current transports warmer water from the western Pacific warm pool to the ETP region. Between the SEC and the NECC there is a narrow equatorial front (EF) that separates warm low-salinity waters in

the north from cool high-salinity waters in the south (Fig. 1; Strub et al., 1998). This front is observable from July to September at about 2.5°N with a strong meridional SST gradient. In contrast, the EF position is unclear from January to April, when the southeast trades winds collapse and SST south of the Equator increases owing to reduced upwelling. The condition of the EF is correlated with the displacement of the intertropical convergence zone (ITCZ) (e.g., Pak and Zaneveld, 1974; Chelton et al., 2001; Raymond et al., 2004). The ITCZ reaches its northernmost extent in the month of August (~12°N) when southeast trade winds are stronger; the ITCZ is located closest to the equator in April (~2°N) when northeast trade winds are stronger (Waliser and Gautier, 1993).

The most influential subsurface current in this region is the EUC that flows eastward beneath the SEC. The EUC is fed by the saline New Guinea Coastal Undercurrent at its the western boundary (Talley et al., 2011) and flows within the equatorial thermocline and shoal as it approaches the Galapagos Islands (Kessler, 2006). When it reaches the Galapagos Islands, it splits into two branches (Steger et al., 1998) with the main branch flowing southward to merge with the Peruvian Undercurrent, which provides a for source of the Peru coastal upwelling (Brink et al., 1983), the other branch continues to flow eastward, merging with the NECC (Wyrtki, 1967; Fieldler and Tally, 2006; Kessler, 2006).

The EEP is a region that has been impacted by coastal upwelling. Coastal upwelling in the EEP is driven by Ekman transport generated by southeast trade winds that blow along the west coast of South America (Wrytki, 1981). The Ekman transport moves surface water offshore, away from the coastal boundary and replaces it with water from below the thermocline to maintain the mass balance. Seasonally, coastal upwelling

93 is at its highest intensity when the strongest southeast trade winds blow over this region
94 in boreal summer, and is reduced when southeast trade winds are relatively weak in
95 boreal winter (Wrytki, 1975, 1981; Kessler, 2006). The seasonal variability in the EEP is
96 superimposed by interannual El Niño events (Wang and Fiedler, 2006), which occur
97 every 2–7 years and last for 6–18 months (Penington et al., 2006). Hydrological
98 conditions that characterize El Niño (La Niña) phases in the EEP are a deeper (shallower)
99 thermocline and weaker (stronger) upwelling (Kessler, 2006).

100 Modern observation shows a clear seasonal and interannual SST variability in the
101 EEP region (Fig. 2a). Seasonally, higher SST is recorded during boreal winter (February),
102 and the lowest SST is recorded in boreal summer (August). The vertical temperature
103 gradient is larger in boreal winter than that in boreal summer. Interannually, higher SST
104 is observed in strong El Niño years and lower SST is observed in strong La Niña years
105 (Fig. 2a). The thermocline depth at the study site is approximately 30–50 m (Fig. 2b).
106

107 **2. Materials and methods**

108 ODP Site 1239 (0º40.32′ S, 82º4.86′ W; 1414 m water depth) is located near the
109 eastern crest of the Carnegie Ridge and ~120 km off the coast of Ecuador (Fig. 1). The
110 sediments are dominated by light to dark olive gray foraminifera-nannofossil ooze with
111 varying amounts of diatoms, clay, and micrite (Mix et al., 2003). The age-depth model of
112 this core was established by Rincon-Martinez et al. (2010) based on correlation of the
113 $\delta^{18}O$ record of the benthic foraminifera *Cibicidoides wuellerstorfi* with the LR04 global
114 stack (Lisiecki and Raymo, 2005). In total, 236 samples were taken from 0.02 to 14.73
115 meters composite depth (mcd) at 2–10 cm intervals.

Extraction and separation of lipids followed the modified method of Yamamoto et al. (2000) and Yamamoto et al. (2008). Freeze-dried and homogenized samples (~2 g) were extracted using an Accelerated Solvent Extractor 200 (ASE 200, DIONEX) with a mixture of dichloromethane and methanol (6/4 v/v) at 100°C. The extract was separated into four fractions of lipid sequences in order of polarity, F1 (3 ml hexane), F2 (3 ml 3/1 v/v hexane–toluene), F3 (4 ml toluene), and F4 (3 ml 3/1 v/v toluene–methanol), by column chromatography (SiO_2 with 5% distilled water; i.d., 5.5 mm; length, 45 mm).

The F3 fraction was analyzed with a Hewlett–Packard Model 6890 gas chromatograph with on-column injection and electronic pressure control inlet systems and a flame ionization detector (FID). Helium was used as carrier gas with the flow velocity maintained at 30 $cm.s^{-1}$. The column was a Chrompack CP-Sil5CB capillary (60 m; i.d., 0.25 mm; thickness, 0.25 µm). The oven temperature was programmed from 70 to 290°C at 20°C min^{-1}, from 290 to 310°C at 0.5°C min^{-1}, and then held for 30 min. Quantification of di- and tri-unsaturated C_{37} alkenones were achieved by comparing the peak areas with that of an internal standard (*n*-$C_{36}H_{74}$) on the gas chromatogram.

The alkenone unsaturation index U^K_{37}' was computed from the concentrations of di-unsaturated ($C_{37:2}$MK) and tri-unsaturated ($C_{37:3}$MK) alkenones using the following equation by Prahl et al. (1988):

$$U^K_{37}' = [C_{37:2}MK] / ([C_{37:3}MK] + [C_{37:2}MK])$$

The temperature was calculated according to an equation derived by Prahl et al. (1988) based on experimental results for cultured strain 55a of *Emiliania huxleyi*:

$$U^{K}_{37}' = 0.034T + 0.039$$

where T = temperature (°C). Analytical accuracy was 0.24°C in our laboratory.

An aliquot of F4 was dissolved in hexane-2-propanol (99/1, v/v). GDGTs were analyzed using high-performance liquid chromatography–mass spectrometry (HPLC-MS) with an Agilent 1100 HPLC system connected to a Bruker Daltonics micrOTOF-HS time-of-flight mass spectrometer. Separation was conducted using a Prevail Cyano column (2.1 x 150 mm, 3μm; Alltech) maintained at 30°C following the method of Hopmans et al. (2000) and Schouten et al. (2007). Detection was achieved by atmospheric pressure positive ion chemical ionization–mass spectrometry (APCI-MS) with full scan mode (m/z 500–1500). Compounds were identified by comparing mass spectra and retention times with those of GDGT standards (formed from the main phospholipids of *Thermoplasma acidophilum* via acid hydrolysis).

Quantification was achieved by integrating the summed-peak areas in the $(M+H)^+$ and the isotopic $(M+H+1)^+$ ion traces and comparing these to the peak area of an internal standard (C_{46} GDGT) in the $(M+H)^+$ ion trace, following to the method of Huguet et al. (2006). The correction value of ionization efficiency between GDGTs and the internal standard was obtained by comparing the peak areas of *T. acidophilum*-derived mixed GDGTs and C_{46} GDGT of known amounts. The standard deviation of a replicate analysis was 3.0% of the concentration for each compound. Concentration TEX_{86}^{H} (applicable in warm water) were calculated from the concentrations of GDGT-1, GDGT-2,

GDGT-3, and a regioisomer of crenarchaeol using the following expressions (Schouten et al., 2002; Kim et al., 2010):

$$TEX_{86} = ([GDGT\text{-}2] + [GDGT\text{-}3] + [Crenarchaeol\ regioisomer]) / ([GDGT\text{-}1] + [GDGT\text{-}2] + [GDGT\text{-}3] + [Crenarchaeol\ regioisomer])$$

$$TEX_{86}^{H} = \log (TEX_{86})$$

Temperature was calculated according to the following equation based on a global core-top calibration (Kim et al., 2010):

$$T = 68.4TEX_{86}^{H} + 38.6 \text{ (when } T > 15°C)$$

where T = temperature (°C). The analytical accuracy was 0.45 °C in our laboratory.

3. Results

3.1 GDGTs and TEX_{86}

The isoprenoid GDGTs detected in ODP 1239 sediments consist of caldrachaeol (GDGT-0), GDGT-1, GDGT-2, GDGT-3, crenarchaeol, and its regioisomer (Appendix I). The total concentration of isoprenoid GDGTs in sediment varied between 0.6 and 12.8 $\mu g.g^{-1}$ with an average of 5.81 $\mu g.g^{-1}$ (Fig. 3b). The relative abundances of different isoprenoid GDGTs were nearly uniform with range of 37–54% for crenarchaeol, 26–35% for caldarchaeol and 15–35% for others.

184 The TEX_{86}^{H}-derived temperature of the core-top sample (25.1°C) agreed with the
185 mean annual SST at the study site (24.5°C, Locarnini et al., 2010). TEX_{86}^{H}-derived SST
186 varied between 20.2 and 27.2°C and was generally higher during interglacials and lower
187 during glacials (Fig. 3a).

188 The branched isoprenoid tetraether (BIT) index, an indicator of soil bacteria
189 contribution (see Hopmans et al., 2004), varied between 0.01 and 0.06 (Fig. 3d)
190 suggesting a low contribution of soil organic matter in the study samples. Weijers et al.
191 (2006) noted that samples having high BIT (>0.4) may show anomalously high TEX_{86}^{H}-
192 derived temperatures, but this concern was not relevant for the samples used in this study.
193
194 *3.2. Alkenones and U^{K}_{37}'*

195 The total concentration of C_{37}-C_{39} alkenones in sediment varied between 0.5 and
196 28.7 $\mu g.g^{-1}$ with an average of 8.9 $\mu g.g^{-1}$ (Fig. 3b). The alkenone concentration tended to
197 be higher in the interval between 400 ka and 240 ka than in the intervals between 430 and
198 400 ka and between 240 and 0 ka.

199 The U^{K}_{37}'-derived temperature of the core-top sample (25.6°C) agreed with the
200 mean annual SST. U^{K}_{37}'-derived SST varied between 21.5 and 26.6°C and was generally
201 higher in interglacials and lower in glacials (Fig. 3a). The U^{K}_{37}' record obtained in this
202 study was nearly identical to a record for the study site by Rincon-Martinez et al. (2010).
203
204 **4. Discussion**
205 **4.1. Difference in proxy-derived temperatures**

206 The variation of TEX_{86}^{H}-derived temperature is roughly consistent with those of
207 the U^{K}_{37}'-derived temperature at the study site (Fig. 3a), but significant difference was
208 observed in the intervals of late MIS 11, and MIS 10, and MIS-6 when the U^{K}_{37}'-derived
209 temperature was a maximum of 5.5°C higher than the TEX_{86}^{H}-derived temperature (Fig.
210 3a).

211 Dubois et al. (2009) and Kienast et al. (2012) assumed that U^{K}_{37}' reflects mean
212 annual SST because the U^{K}_{37}'-derived temperature in EEP core-top sediments
213 corresponded to mean annual SST. A sediment trap study at two sites in the central
214 tropical Pacific showed no significant difference in the sinking flux of alkenone
215 producers (*Emiliania huxleyi* and *Gephyrocapsa oceanica*) between strong and weak El
216 Niño periods (Broerse, 2000), suggesting that the production of alkenone is not sensitive
217 to upwelling intensity. We thus assume that U^{K}_{37}' does reflect the mean annual SST at the
218 study site.

219 The behavior of Thaumarchaeota and the production of GDGTs are not fully clear
220 in the EEP. Thaumarchaeota (GDGTs producer) are ubiquitous and abundant throughout
221 the seawater column (e.g., Massana et al., 2000; Karner et al., 2001). In the central
222 equatorial Pacific, GDGTs are mainly produced in the thermocline layer (TL) (Turich et
223 al., 2007). Recent case studies assumed that the TEX_{86}^{H}-derived temperatures in EEP
224 sediments reflect the temperature of the thermocline (30–50 m) rather than SSTs (Ho et
225 al., 2011; Seki et al., 2012). Thaumarchaeota in marine environments have been
226 recognized to be both heterotrophs (e.g., Ouverney and Fuhrman, 2000; Agogué et al.,
227 2008; Zhang et al., 2009) and chemoautotrophic nitrifiers (e.g., Könneke et al., 2005;
228 Hallam et al., 2006). Organic matter and NH_3 are produced by phytoplankton and by the

decay of organic matter in surface and subsurface water, which explains why Thaumarchaeota are produced in both the surface mixed layer (SML) and TL. We thus assume that TEX_{86}^{H} reflects a mixed temperature signal from the SML and TL (Fig.4). The production of Thaumarchaeota is fueled by the supply of organic matter and NH_3. Both are more enhanced by phytoplankton production in upwelling periods. Yamamoto et al. (2012) observed that enhanced sinking flux of GDGTs is linked with phytoplankton bloom in the mid-latitude northwestern Pacific. GDGT abundance thus may reflect primary production and upwelling intensity.

TEX_{86}^{H} showed higher temperatures than U^{K}_{37}' during the some deglaciations (Fig. 3a), but this does not mean that the integrated SST of the SML and TL was higher than the SST of the SML. The calibration of TEX_{86}^{H} to SST was conducted by comparing core-top TEX_{86}^{H} with mean annual SST (Kim et al., 2010). If the phenomenon of TEX_{86}^{H} recording both the SST and thermocline temperatures is common in tropical oceans, then calibration requires a comparison between core top TEX_{86}^{H} and integrated temperatures of the SML and TL; this calibration should give cooler estimates. The temperature reversal during the last deglaciation is thus attributed to the overestimation of TEX_{86}^{H}-derived temperature.

4.2. GDGT/alkenone ratio and ΔT as upwelling indices

The relative abundance of isoprenoid GDGTs to alkenones (GDGT/alkenone ratio) was enhanced during the last five deglaciations (Fig. 5a), suggesting an enhanced production of GDGTs. When upwelling intensifies, GDGT production increases due to increasing NH_3 and organic matter. In contrast, when upwelling weakens, GDGT

252 production decreases. The GDGT/alkenone ratio can thus be used as an index of
253 upwelling intensity.

254 The difference between TEX_{86}^{H}- and U^{K}_{37}'-derived temperatures (ΔT) was
255 computed by subtracting U^{K}_{37}'-derived SST from TEX_{86}^{H}-derived temperature (ΔT =
256 $TEX_{86}^{H} - U^{K}_{37}'$). U^{K}_{37}' reflects the temperature of the SML and TEX_{86}^{H} reflects
257 integrated temperatures from the SML and the TL. When upwelling intensifies, the
258 temperature gradient between the SML and TL decreases (Fig. 4), and ΔT shifts in a
259 positive direction. In contrast, when upwelling weakens, the temperature gradient
260 between the SML and TL increases, and ΔT shifts in a negative direction. We thus
261 assume that ΔT is a potential index of upwelling intensity.

262 ΔT varied between -6.2 and 4.1°C and showed maxima at 15, 50, 127, 213, 243,
263 260, 274, 310, 330, 340 and 427 ka. The maxima at 15, 127, 243, 340, and 427 ka
264 correspond to glacial terminations (Fig. 5a). Minimal peaks of ΔT occurred at 33, 86, 179,
265 237, 289, and 386 ka. The variation in ΔT is very similar to that in the GDGT/alkenone
266 ratio, although there are some mismatches in MIS 8 and MIS 11. This correspondence
267 suggests that both are robust indices of upwelling intensity.

268 Positive ΔT and an elevated GDGT/alkenone ratio at the study site during
269 deglaciations are associated with heavier $\delta^{18}O$ of subsurface-dwelling foraminifera (Pena
270 et al., 2008) and increased export production (Pedersen, 1983; Lyle et al., 1988; Kienast
271 et al., 2006) in the EEP. Pena et al. (2008) showed that thermocline water $\delta^{18}O$ (DT-
272 $\delta^{18}O_{sw}$) at ODP Site 1240, reconstructed from the subsurface-dwelling foraminifera
273 *Neogloboquadrina dutertrei*, was maximized during the last three deglaciations (Fig. 5d).
274 This suggests intensified upwelling in those periods. Abrupt increases in organic carbon

content during deglaciations were reported from sites P6 (Pedersen, 1983), V19-28 (Lyle et al., 1988), and ME0005A-24JC and 27JC (Kienast et al., 2006) in the EEP (Fig. 5b), suggesting that export production was maximized during the last two deglaciations. The elevated ΔT and GDGT/alkenone ratio at the study site indicate not only the intensification of local upwelling, but also the intensification of regional upwelling associated with thermocline shoaling and enhanced export production in the EEP during deglaciations.

4.3. Hydrological evolution in the EEP

The ΔT record mirrors sedimentary $\delta^{15}N$ records from the Peru margin (Fig. 5c), which have been suggested to reflect the intensity of denitrification regulated by Peruvian coastal upwelling (Ganeshram et al., 2000). The trend in $\delta^{15}N$ at the Peru margin was slightly different from those in the EEP (Dubois and Kienast, 2011) and at the Mexican margin (Ganeshram et al., 2000) (Fig. 5c). The maxima of $\delta^{15}N$ at terminations are significant at the Peru margin but not in the EEP or at the Mexican margin, suggesting that $\delta^{15}N$ in the eastern Pacific margin was determined by the denitrification in the Peru margin and modified by local factors (Robinson et al., 2009). The correspondence between ΔT and the Peru margin $\delta^{15}N$ records suggests that the upwelling at the study site was closely linked with Peruvian coastal upwelling. The study site is located in a region influenced by the coastal upwelling system (Wrytki, 1981; Pennington et al., 2006; Talley et al., 2011). Because the southeast trade winds are a principal agent driving coastal upwelling along the west coast of South American continent (Wrytki, 1981;

297 Kessler, 2006), it is highly likely that the southeast trade winds intensified during
298 deglaciations owing to the stronger South Pacific High.

299 The paleo-position of the ITCZ was approximated using dust fluxes across the
300 equator over the last 30 ka (McGee et al., 2007). The results of that analysis suggest that
301 the ITCZ did not shift southward during the last deglaciation. Xie and Marcantonio
302 (2012) precisely estimated the paleo-position of the ITCZ using neodymium isotopes
303 (ε_{Nd}) derived from transect dust obtained by McGee et al. (2007). The average ε_{Nd} values
304 from the last glacial and Holocene show similar gradients throughout the equatorial
305 transect, but the latitudinal gradient was stronger, and a steeper interval was evident
306 during the last deglaciation between 5°N and 7°N. This suggests more northerly mean
307 position of the ITCZ.

308 Yamamoto et al. (2007) reconstructed the intensity of the California Current
309 during the last 150,000 years and showed that the subtropical high-pressure cell in the
310 North Pacific weakened during the last two deglaciations. Lyle et al. (2012) suggested
311 that high precipitation in the Great Basin of the western United States during the last
312 deglaciation was not caused by the southward shift of westerly storms, but instead by the
313 northward transport of moist air masses from the tropical Pacific because of the weaker
314 North Pacific High. This presumes that the northeast trade winds were not intensified
315 under the condition of the weaker North Pacific High.

316 The stronger South Pacific High, combined with the weaker North Pacific High
317 and northward shift of the ITCZ during the last deglaciation was an asymmetrical
318 atmospheric phenomenon between the Northern and Southern hemispheres. This anti-
319 phase variation in the subtropical high-pressure cells of both hemispheres was

presumably caused by changes in the heat balance between the hemispheres (Fig. 6).

The ENSO model has been applied to understand hydrological evolution of the EEP (e.g., Lea et al., 2000; Koutavas et al., 2002; Koutavas and Lynch-Stieglitz, 2003; Martinez et al., 2003; Pena et al., 2008; Rincon-Martinez et al., 2010). Pena et al. (2008) proposed the deep thermocline seawater $\delta^{18}O$ (DT-$\delta^{18}O_{sw}$) based on *Neogloboquadrina dutertrei* $\delta^{18}O$ at Site 1240 and suggested that EEP hydrology was characterized by a La Niña-like condition during deglaciations. However, the zonal gradient of SST was inconsistent with a La Niña-like state during the last deglaciation (Fig. 5e). The DT-$\delta^{18}O_{sw}$ at ODP Site 1240 showed maximum peaks during deglaciations (Pena et al., 2008), but the Mg/Ca-SST, between the western and eastern Pacific did not show a large temperature gradient typical of La Niña (Lea et al., 2000). Also, the weaker North Pacific High evidenced during the last deglaciation (Yamamoto et al., 2007; Lyle et al., 2012) is not consistent with a La Niña-like state; a weaker North Pacific High is typical of the modern El Niño condition (Bogad and Lynn, 2001). We thus suggest that intensified upwelling shown by enhanced DT-$\delta^{18}O_{sw}$ at Site 1240 was not linked to a La Niña-like state, and an ENSO analogy cannot to be applied to explain hydrological conditions in the Pacific during the last deglaciation.

The intensification of upwelling in the EEP and the Peru margin during the last deglaciation coincided with intensification of upwelling in the Southern Ocean (Toggweiler et al., 2006; Anderson et al., 2009). Because upwelling in the Southern Ocean is regulated by the position of the southern westerlies (Russell et al., 2006; Toggweiler et al., 2006), the synchronous intensification of upwelling systems in the EEP, the Peru margin, and the Southern Ocean suggests that the reorganization of atmospheric

circulation in the Southern Hemisphere induced the intensification of the subtropical high-pressure cell, causing stronger southeast trade winds along the west coast of South America and southern westerlies over the Southern Ocean, enhancing upwelling in both regions.

The intensification of the South Pacific High caused southern westerlies to move poleward and the ITCZ to shift northward during deglaciations (Fig. 6). In response, the center of upwelling moved northward and cold tongue upwelling in the EEP area intensified. The stronger South Pacific High during the last deglaciation caused a drier climate in the Patagonia region of South America (de Porras et al., 2012), and the weaker North Pacific High caused a wetter climate in the Great Basin of the western United States (Lyle et al., 2012). This perspective is useful for understanding the hydrological and climatological evolution of the eastern Pacific region.

5. Conclusions

The abundance ratio of GDGTs to alkenone (GDGT/alkenone ratio) and difference between TEX_{86}^{H}- and U^{K}_{37}'-derived temperature (ΔT) can be used as upwelling indices in the EEP. Our new data show that intensification of upwelling occurred in the EEP at each of the last five glacial terminations. The result suggests that the intensification of upwelling was a common phenomenon in the EEP at glacial terminations. The similar timing of intensified upwelling in the EEP, the Peru margin, and the Southern Ocean suggests an intensification of the South Pacific High during deglaciations. This new perspective can help explain the hydrological evolution of the eastern Pacific region during deglaciations.

Acknowledgements

The Ocean Drilling Program Leg 202 provided the samples used in this study. We thank Daniel Rincon Martinez for providing us with data on the age and foraminiferal oxygen isotopes of the study core. We also thank Patrizia Ziveri, Alexandra Broerse, and Kyoko Hagino for providing information on coccolithophores in the EEP, Leopoldo Pena for data regarding the thermocline water $\delta^{18}O$ from ODP Site 1240, Eric Galbraith for data of $\delta^{15}N$ records from core NH22P and CD38-02, and Tatsufumi Okino, Keiko Ohnishi and Tadamichi Oba for their analytical assistance.

References

Agogué, H., Brink, M., Dinasquet, J., Herndl, G.J., 2008. Major gradients in putatively nitrifying and non-nitrifying Archaea in the deep North Atlantic. Nature 456, 788–792.

Anderson, R.F., Ali, S., Bradtmiller, L.I., Nielsen, S.H.H., Fleisher, M.Q., Anderson, B.E., Burckle, L.H., 2009. Wind-driven upwelling in the Southern Ocean and the deglacial rise in atmospheric CO_2. Science 323, 1443–1448.

Beaufort, L., de Garidel-Thoron, T., Mix, A.C., Pisias, N.G., 2001. ENSO-like forcing on oceanic primary production during the late Pleistocene. Science 293, 2440–2444.

Bograd, S., Lynn, R.J., 2001. Physical-biological coupling in the California Current during the 1997–99 El Niño-La Niña cycle. Geophysical Research Letters 28, 275–278.

Brink, K.H., Halpern, D., Huyer, A., Smith, R.L., 1983. The physical environment of the

389 Peruvian upwelling system. Progress in Oceanography 12, 285–305.
390 Broerse, A.T.C., 2000. Coccolithophore export production in the selected ocean
391 environments, Ph.D. thesis, Faculty of Earth Science, Vrije Universiteit, Amsterdam,
392 Netherlands.
393 Chelton, D.B., Esbensen, S.K.. Schlax, M.G., Thum, N., Freilich, M.H., Wentz, F.J.,
394 Gentemann, C.L., McPhaden, M.J. Schopf, P.S., 2001. Observations of coupling
395 between surface wind stress and sea surface temperature in the eastern tropical
396 Pacific. Journal of Climate 14, 1479–1498.
397 de Porras, M.E., Maldonado, A, Abarzúa, A.M., Cárdenas, M.L., Francois, J.P., Martel-
398 Cea, A., Stern, C.R., Méndez, C., Reyes, O., 2012. Postglacial vegetation, fire and
399 climate dynamics at Central Chilean Patagonia (Lake Shaman, 44°S). Quaternary
400 Science Reviews 50, 71–85.
401 Dubois, N., Kienast, M., Normandeau, C. Herbert, T.D., 2009. Eastern equatorial
402 Pacific cold tongue during the last glacial maximum as seen from alkenone
403 paleothermometry. Paleoceanography 24, PA4207.
404 Dubois, N., Kienast, M., 2011. Spatial reorganization in the equatorial divergence in the
405 eastern tropical Pacific during the last 150 kyr. Geophysical Research Letters 38,
406 L16606.
407 Fiedler, P.C., Lavin, M.F., 2006. Introduction: a review of eastern tropical Pacific
408 oceanography. Progress in Oceanography 69, 94–100.
409 Fiedler, P.C., Talley, L.D., 2006. Hydrography of the eastern tropical Pacific: a review.
410 Progress in Oceanography 69 (2–4), 143–180.

411 Ganeshram, R.S., Pedersen, T.F., Calvert, S.E., McNeil, G.W., Fontugne, M.R., 2000.
412 Glacial-interglacial variability in denitrification in the world's oceans: causes and
413 consequences. Paleoceanography 15, 361–376.
414 Hallam, S.J., Mincer, T.J., Schleper, C., Preston, C.M., Roberts, K., Richardson, P.M.,
415 DeLong, E.F., 2006. Pathway of carbon assimilation and ammonia oxidation
416 suggested by environmental genomic analyses of marine Crenarchaeota. PLoS
417 Biology 4, 520–536.
418 Ho, S. L., Yamamoto, M., Mollenhauer, G., Minagawa M., 2011. Core top TEX_{86} values
419 in the south and equatorial Pacific. Organic Geochemistry 42, 94–99.
420 Hopmans, E.C., Schouten, S., Pancost, R., van der Meer, M.T.J., Sinninghe Damsté, J.S.,
421 2000. Analysis of intact tetraether lipids in archaeal cell material and sediments by
422 high performance liquid chromatography/atmospheric pressure chemical ionization
423 mass spectrometry. Rapid Communications in Mass Spectrometry 14, 585–589.
424 Hopmans E.C., Weijers, J.W.H., Schefuß, E., Herfort, L., Sinninghe Damsté, J.S.,
425 Schouten, S., 2004. A novel proxy for terrestrial organic matter in sediments based
426 on branched and isoprenoid tetraether lipids. Earth and Planetary Science Letters 224,
427 107–116.
428 Huguet, C., Hopmans, E.C., Febo-Ayala, W., Thompson, D.H., Sinninghe Damsté, J.S.,
429 Schouten, S., 2006. An improved method to determine the absolute abundance of
430 glycerol dibiphytanyl glycerol tetraether lipids. Organic Geochemistry 37, 1036–
431 1041.
432 Imbrie, J., Boyle, E.A., Clemens, S.C., Duffy, A., Howard, W.R., Kukla, G., Kutzbach, J.,
433 Martinson, D.G., McIntyre, A., Mix, A.C., Molfino, B., Morley, J.J., Peterson, L.C.,

Pisias, N.G., Prell, W.L., Raymo, M.E., Shackleton, N.J., Toggweiler, J.R., 1992. On the structure and origin of major glaciation cycles. I. Linear responses to Milankovitch forcing. Paleoceanography 7, 701–738.

Karner, M.B., DeLong, E.F., Karl, D.M., 2001. Archaeal dominance in the esopelagic zone of the Pacific Ocean. Nature 409, 507–510.

Kessler, W.S., 2006. The circulation of the eastern tropical Pacific: a review. Progress in Oceanography 69, 181–217.

Kienast, M., Kienast, S., Calvert, S., Eglinton, T., Mollenhauer, G., Francois, R., Mix, A., 2006. Eastern Pacific cooling and Atlantic overturning circulation during the last deglaciation. Nature 443, 846–849.

Kienast, M., MacIntyre, G., Dubois, N., Higginson, S., Normandeau, C., Chazen C.R., 2012. Alkenone unsaturation in surface sediments from the eastern equatorial Pacific: Implications for SST reconstructions. Paleoceanography 27, PA1210.

Kim, J.H., van der Meer, J., Schouten, S., Helmke, P., Willmott, V., Sangiorgi, F., Koc, N., Hopmans, E.C., Sinninghe Damsté, J.S., 2010. New indices and calibrations derived from the distribution of crenarchaeol isoprenoid tetraether lipids: implications for past sea surface temperature reconstructions. Geochimica et Cosmochimica Acta 74, 4639–4654.

Könneke, M., Bernhard, A.E., de la Torre, J.R., Walker, C.B., Waterbury, J.B., Stahl, D.A., 2005. Isolation of an autotrophic ammonia-oxidizing archaeon. Nature 437, 543–546.

455 Koutavas, A., Lynch-Stieglitz, J., 2003. Glacial-interglacial dynamics of the eastern
456 equatorial Pacific cold tongue. Intertropical Convergence Zone system reconstructed
457 from oxygen isotope records. Paleoceanography 18, 1089.
458 Koutavas, A., Lynch-Stieglitz, J., Marchitto, T.M., Sachs, J.P., 2002. El Niño-like pattern
459 in ice age tropical Pacific sea surface temperature. Science 297, 226–230.
460 Lea, D.W., Pak, D.K., Spero, H.J., 2000. Climate impact of late quaternary equatorial
461 Pacific sea surface temperature variations. Science 289, 1719–1724.
462 Lisiecki, L.E., Raymo, M.E., 2005. A Pliocene-Pleistocene stack of 57 globally
463 distributed benthic $\delta^{18}O$ records. Paleoceanography 20, PA1003.
464 Locarnini, R.A., Mishonov, A.V., Antonov, J.I., Boyer, T.P., Garcia, H.E., Baranova, O.
465 K., Zweng, M.M., Johnson, D.R., 2010. In: Levitus, S. (Ed.), World Ocean Atlas
466 2009, 1, Temperature, NOAA Atlas NESDIS, 68, U.S. Government Printing Office,
467 Washington, D.C., pp. 184.
468 Lyle, M., Murray, D.W., Finney, B.P., Dymond, J., Pobbins, J.M., Brooksforce, K., 1988.
469 The record of Late Pleistocene biogenic sedimentation in the eastern tropical Pacific
470 Ocean. Paleoceanography 3, 39–59.
471 Lyle, M., Prahl, F.G., Sparrow M.A., 1992. Upwelling and productivity changes inferred
472 from a temperature record in the central equatorial Pacific. Nature 355, 812–815.
473 Lyle, M., Heusser, L., Ravelo, C., Yamamoto, M., Barron, J., Diffenbaugh, N.S., Herbert,
474 T., Andreasen, D., 2012. Out of the Tropics: The Pacific, Great Basin Lakes, and
475 Late Pleistocene water cycle in the western United States. Science 337, 1629–1633.

476 Martinez, I., Keigwin, L., Barrows, T.T., Yokoyama, Y., Southon, J., 2003. La Niña-like
477 conditions in the eastern equatorial Pacific and a stronger Choco jet in the northern
478 Andes during the last glaciations. Paleoceanography 18, 1033.
479 Massana, R., Delong, E. F., Pedros-Alio, C., Murray, A. E. Preston, C. M. ,2000. A few
480 cosmopolitan phylotypes dominate planktonic archaeal assemblages in widely
481 different oceanic provinces. Applied of Environmental Microbiology 66, 1777–1787.
482 Medina-Elizalde, M., Lea, D.W., 2005. The Mid-Pleistocene transition in the tropical
483 Pacific. Science 310, 1009–1012.
484 McGee, D., Marcantonio F., Lynch-Stieglitz, J., 2007. Deglacial changes in dust flux into
485 the eastern equatorial Pacific. Earth and Planetary Science Letters 257, 215–230.
486 Mix, A.C., Tiedemann, R., Blum, P., et al., 2003. Proceeding of the Ocean Drilling
487 Program, Initial Reports, 202: College Station, TX (Ocean Drilling Program), 1–93.
488 Ouverney, C.C., Fuhrman, J.A., 2000. Marine planktonic archaea take up amino acids.
489 Applied Environmental Microbiology 66, 4829–4833.
490 Paillard, D., Labeyrie, L., Yiou, P., 1996. Macintosh program performs time-series
491 analysis. Eos Transaction AGU 77, 379.
492 Pak, H., Zaneveld, J.R.V., 1974. Equatorial front in the eastern Pacific Ocean. Journal of
493 Physical Oceanography 4, 570–578.
494 Pedersen, T.F., 1983. Increased productivity in the eastern equatorial Pacific during the
495 last glacial maximum (19,000 to 14,000 yr. B.P.). Geology 11, 16–19.
496 Pena, L.D., Cacho, I., Ferretti, P., Hall, M.A., 2008. El Niño-Southern Oscillation-like
497 variability during glacial terminations and interlatitudinal tele-connections.
498 Paleoceanography 23, PA3101.

499 Pennington, J.T., Mahoney, K.L., Kuwahara, V.S., Kolber, D.D., Calienes, R., Chavez,
500 F.P., 2006. Primary production in the eastern tropical Pacific: a review. Progress in
501 Oceanography 69 (2 – 4), 285–317.
502 Prahl, F.G., Muehlhausen, L.A., Zahnke, D.L., 1988. Further evaluation of long chain
503 alkenones as indicators of paleoceanographic conditions. Geochimica et
504 Cosmochimica Acta 52, 2303–2310.
505 Raymond, D.J., Esbensen, S.K., Paulson, C., Gregg, M., Bretherton, C.S., Petersen, W.A.,
506 Cifelli, R., Shay, L.K., Ohlmann, C., Zudeima, P., 2004. EPIC2001 and the coupled
507 ocean-atmosphere system of the tropical east Pacific. Bulletin of American
508 Meteorological Society 85, 1341–1354.
509 Reynolds, R.W., Rayner, N.A., Smith, T.M., Stokes, D.C., Wang, W., 2002. An
510 improved in situ and satellite SST analysis for climate. Journal of Climate 15, 1609–
511 1625.
512 <http://iridl.ldeo.columbia.edu/SOURCES/.NOAA/.NCEP/.EMC/.CMB/.GLOBAL/.
513 Reyn_SmithOIv2/.monthly/>
514 Rincon-Martínez, D., Lamy, F., Contreras, S., Leduc, G., Bard, E., Saukel, C., Blaz, T.,
515 Mackensen, A., Tiedeman, R., 2010. More humid interglacials in Ecuador during the
516 past 500 kyr linked to latitudinal shifts of the equatorial front and Intertropical
517 Convergence Zone in the eastern equatorial Pacific. Paleoceanography 25, PA2210.
518 Robinson, R.S., Martinez, P., Pena, L.D., Cacho, I., 2009. Nitrogen isotopic evidence for
519 deglacial changes in nutrient supply in the eastern equatorial Pacific.
520 Paleoceanography 24, PA4213.

Russell, J.L., Dixon, K.W., Gnanadesikan, A., Stouffer, R.J., Toggweiler, J.R., 2006. The Southern hemisphere westerlies in a warming world: propping open the door to the deep ocean. Journal of Climate 19, 6382–6390.

Schouten, S., Hopmans, E.C., Schefuß, E., Sinninghe Damsté, J.S., 2002. Distributional variations in marine crenarchaeotal membrane lipids: a new organic proxy for reconstructing ancient sea water temperatures? Earth and Planetary Science Letters 204, 265–274.

Schouten, S, Hudget, C., Hopmans, E.C., Kienhuis, M.V.M., Sinninghe Damsté, J.S., 2007. Analytical methodology for TEX_{86} paleothermometry by high performance liquid chromatography/atmospheric pressure chemical ionization-mass spectrometry. Analytical Chemistry 79, 2940–2944.

Seki, O., Schmidt, D.N., Schouten, S., Hopmans, E.C., Sinninghe Damsté, J.S., Pancost, R.D., 2012. Paleoceanographic changes in the eastern equatorial Pacific over the last 10 Myr. Paleoceanography 27, PA3224.

Spero, H.J., Lea, D.W., 2002. The cause of carbon isotope minimum events on glacial terminations. Science 296, 522–525.

Steger, J.M., Collins, C.A., Chu P.C., 1998. Circulation in the Archipielago de Colon (Galápagos Islands). Deep-Sea Research II 45, 1093–1114.

Strub, P.T., Mesias, J.M., Montecino, V., Rutllant, J., Salinas, S., 1998. Coastal ocean circulation off western South America. In: Robinson, A.R., Brink, K.H. (Eds.), The Sea, Ideas and Observations on Progress in the Study of the Seas, Vol. 11, Global Coastal Ocean Regional Studies and Syntheses. Wiley, New York, pp. 273–313.

543 Talley, L.D., Pickard, G.L., Emery, W.J., Swift, J.H., 2011. Descriptive physical
544 oceanography. 6th Edition. Elsevier, Boston.
545 Toggweiler, J.R., Russell, J.L., Carson, S., 2006. Midlatitude westerlies, atmospheric
546 CO_2, and climate change during the ice ages. Paleoceanography 21, PA2005.
547 Trenberth, K.E., 1997. The definition of El Niño. Bulletin of the American
548 Meteorological Society 78, 2771–2777.
549 Turich, C., Freeman, K.H., Bruns, M.A., Conte, M., Jones, A.D. and Wakeham, S.G.,
550 2007. Lipids of marine Archaea: Patterns and provenance in the water-column and
551 sediments. Geochimica et Cosmochimica Acta 71, 3272–3291.
552 Waliser, D.E., Gautier, C., 1993, A satellite-derived climatology of the ITCZ. Journal of
553 Climate 6, 2162–2174.
554 Wang, C., Fiedler, P.C., 2006. ENSO variability in the eastern tropical Pacific: a review.
555 Progress in Oceanography 69 (2–4), 239–266.
556 Weijers, J.W.H., Schouten, S., Spaargaren, O.C., Sinninghe Damsté, J.S., 2006.
557 Occurrence and distribution of tetraether membrane in soils: implications for the use
558 of the BIT index and the TEX_{86} SST proxy. Organic Geochemistry 37, 1680–1693.
559 Wyrtki, K., 1967. Circulation and water masses in the eastern equatorial Pacific Ocean.
560 International Journal of Oceanology and Limnology 1, 117–147.
561 Wyrtki, K., 1975. El Niño – The dynamic response of the equatorial Pacific Ocean to
562 atmospheric forcing. Journal of Physical Oceanography 5, 572–584.
563 Wyrtki, K., 1981. An estimate of equatorial upwelling in the Pacific. Journal of Physical
564 Oceanography 11, 1205–1214.

565 Xie, R.C., Marcantonio, F., 2012. Deglacial dust provenance changes in the eastern
566 equatorial Pacific and implications for ITCZ movement. Earth and Planetary Science
567 Letters 317-318, 386–395.
568 Yamamoto, M., Shiraiwa, Y., Inouye, I., 2000. Physiological responses of lipids
569 in *Emiliania huxleyi* and *Gephyrocapsa oceanica* (Haptophyceae) to growth status
570 and their implications for alkenone paleothermometry. Organic Geochemistry
571 31, 799–811.
572 Yamamoto, M., Yamamuro, M., Tanaka, Y., 2007. The California current system during
573 the last 136,000 years: response of the North Pacific High to precessional forcing.
574 Quatenary Science Reviews 26, 405–414.
575 Yamamoto, M., Okino, T., Sugisaki, S., Sakamoto, T., 2008. Late Pleistocene changes in
576 terrestrial biomarkers in sediments from the central Arctic Ocean. Organic
577 Geochemistry 39, 754–763.
578 Yamamoto, M., Shimamoto, A., Fukuhara, T., Tanaka, Y., Ishizaka, J., 2012. Glycerol
579 dialkyl glycerol tetraethers and TEX_{86} index in sinking particles in the western North
580 Pacific. Organic Geochemistry 53, 52–62.
581 Zhang, Y., Sintes, E., Chen, J., Zhnag, Y., Dai, M., Jiao, N., Herndl, G.J., 2009. Role of
582 mesoscale cyclonic eddies in the distribution and activity of Archaea and bacteria in
583 the South China Sea. Aquatic Microbial Ecology 56, 65–79.
584

585 Figure

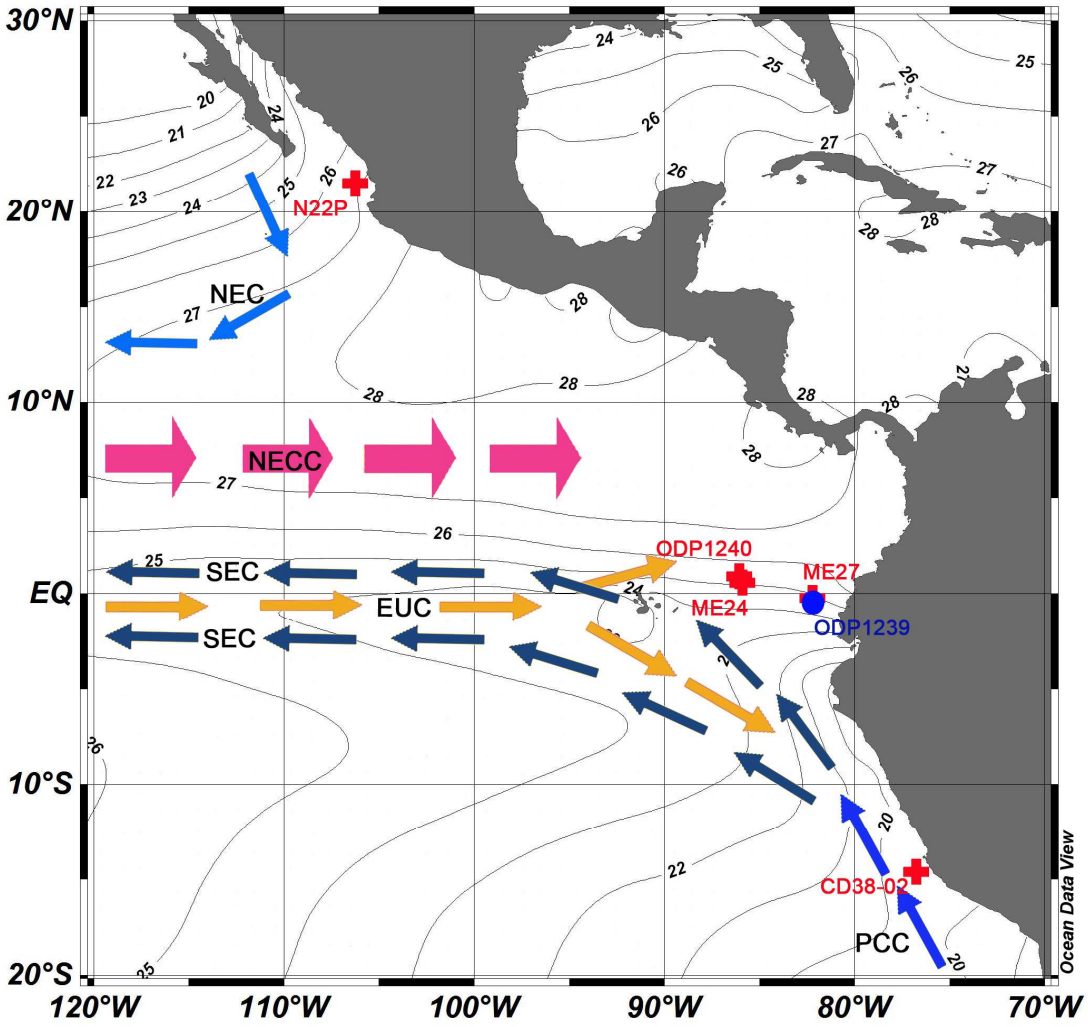

586

587 Figure 1. Map showing mean annual SST (Locarnini et al., 2010), the location of ODP
588 Site 1239 (this study), Sites 1240, ME24, ME27, N22P, CD38-02 and the surface and
589 subsurface ocean currents in the EEP. SEC = South Equatorial Current, NEC = North
590 Equatorial Current, EUC = Equatorial Undercurrent, NECC = North Equatorial
591 Countercurrent; modified after Kessler (2006) and Pennington et al. (2006).

592

593

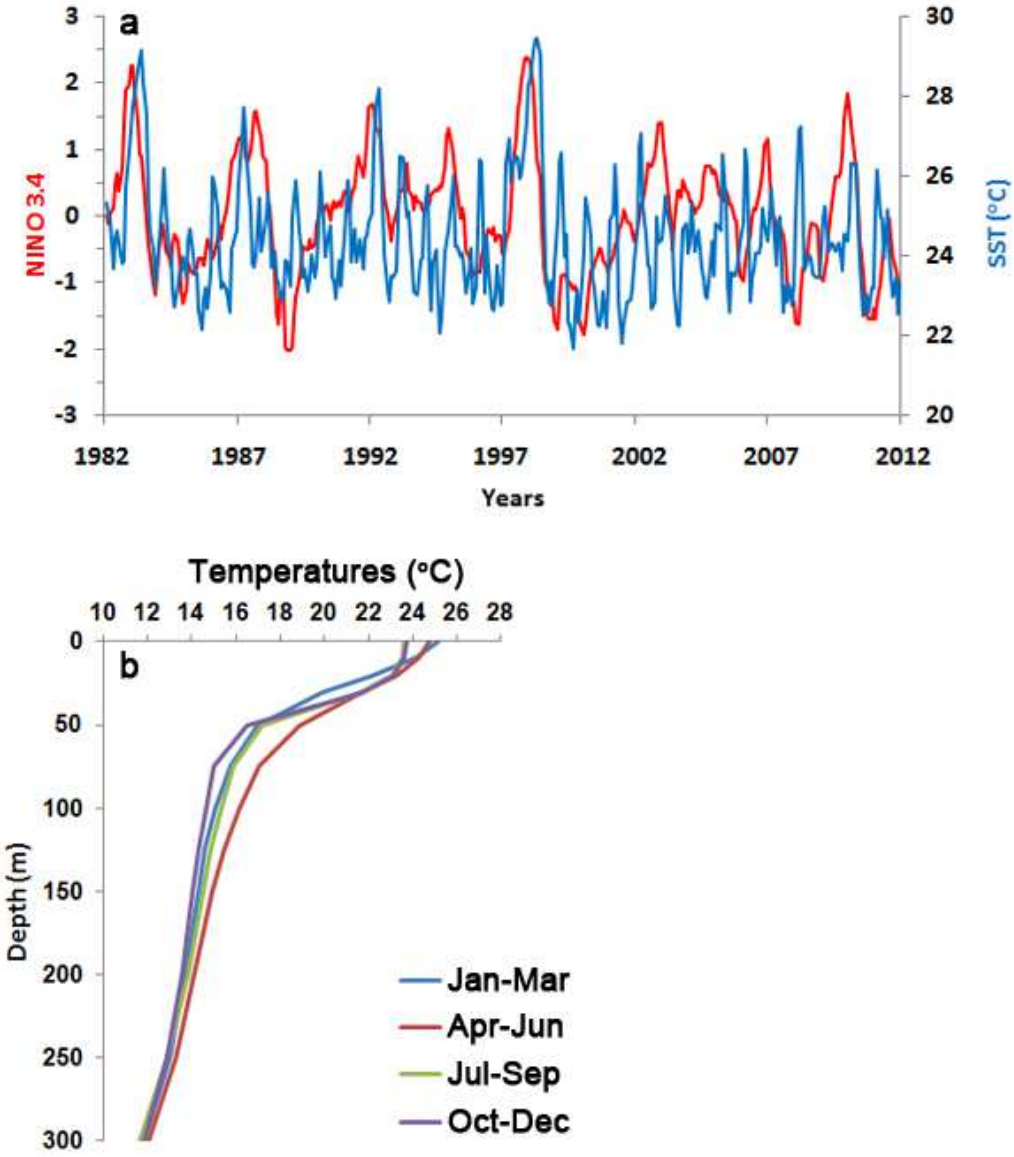

Figure 2. Records of (a) Niño 3.4 index (averaged SST anomaly in the region 170°W–120°W, 5°S–5°N) (Trenberth, 1997) and monthly SST at 0.5°S, 82.5°W (Reynolds et al., 2002) from January 1982 to December 2011 (see online data at http://iridl.ldeo.columbia.edu/SOURCES/.NOAA/.NCEP/.EMC/.CMB/.GLOBAL/.Reyn_SmithOIv2/.monthly/ for detail); (b) Seasonal vertical water structure at 0.5°S, 82.5°W (see online data at http://iridl.ldeo.columbia.edu/SOURCES/.LEVITUS94/.MONTHLY/.temp/)

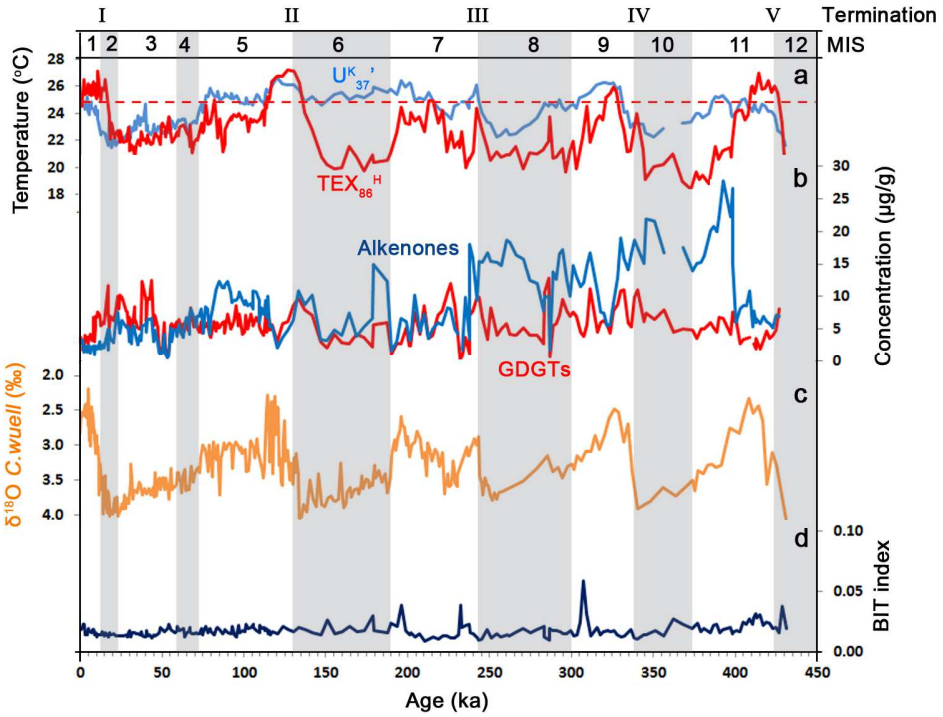

602

603 Figure 3. Variations in (a) TEX_{86}^{H}- and U^{K}_{37}'-derived temperatures; (b) the concentration
604 of alkenones and isoprenoid GDGTs; (c) $\delta^{18}O$ of the benthic foraminifera *C. wuellerstorfi*
605 at the study site (Rincon-Martinez et al., 2010); (d) branched isoprenoid tetraether (BIT)
606 index.

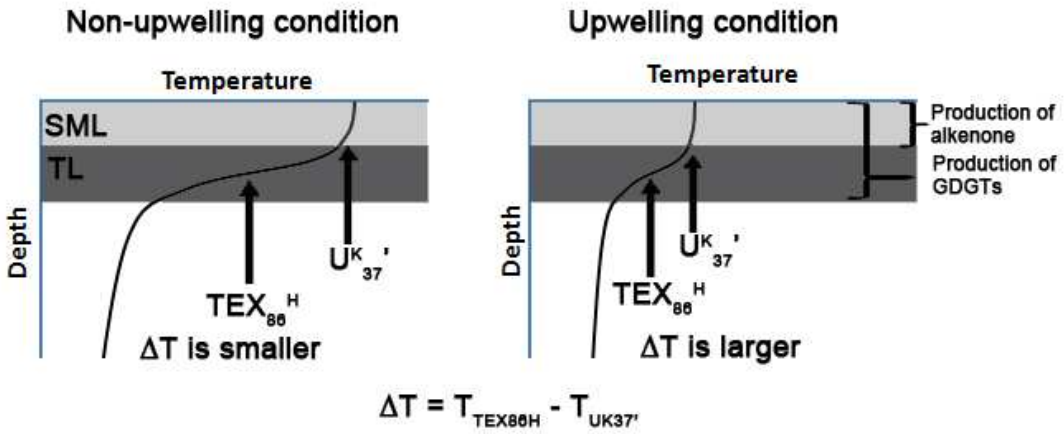

607

608 Figure 4. Conceptual model of ΔT in upwelling and non-upwelling conditions.

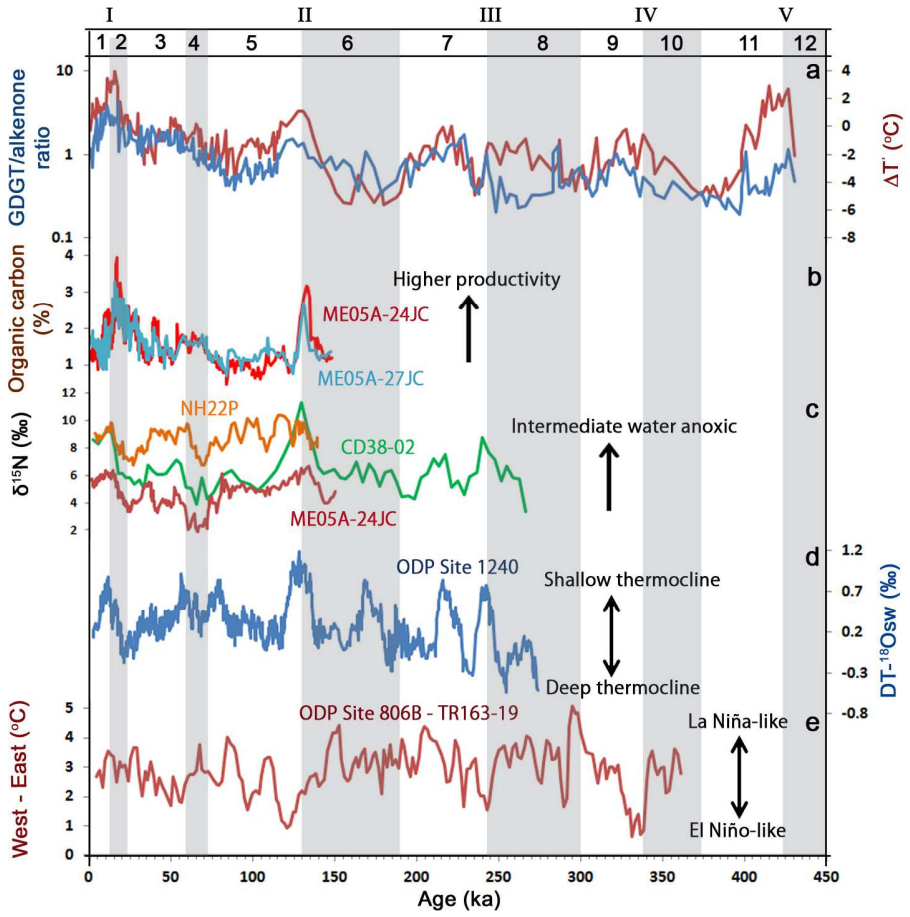

Figure 5. Variation in (a) the difference between TEX_{86}^{H} and U^{K}_{37}' temperatures (ΔT) and the abundance ratio of GDGTs to alkenones (GDGT/alkenone); (b) organic carbon content at ME0005A-24JC and ME0005A-27JC (Dubois and Kienast, 2011); (c) $\delta^{15}N$ of bulk sediments from cores CD38-02 and NH22P at the Peru and Mexican margins, respectively (Ganeshram et al., 2000) and core ME0005A-27JC in the EEP (Dubois and Kienast, 2011); (d) DT-$\delta^{18}O_{sw}$ at ODP Site 1240 (Pena et al., 2008); (e) Mg/Ca-derived temperature difference (smoothed; west-east) between the western equatorial Pacific

(ODP Site 806B; Medina-Elizalde and Lea, 2005) and the EEP (core TR163-19; Lea et al., 2000).

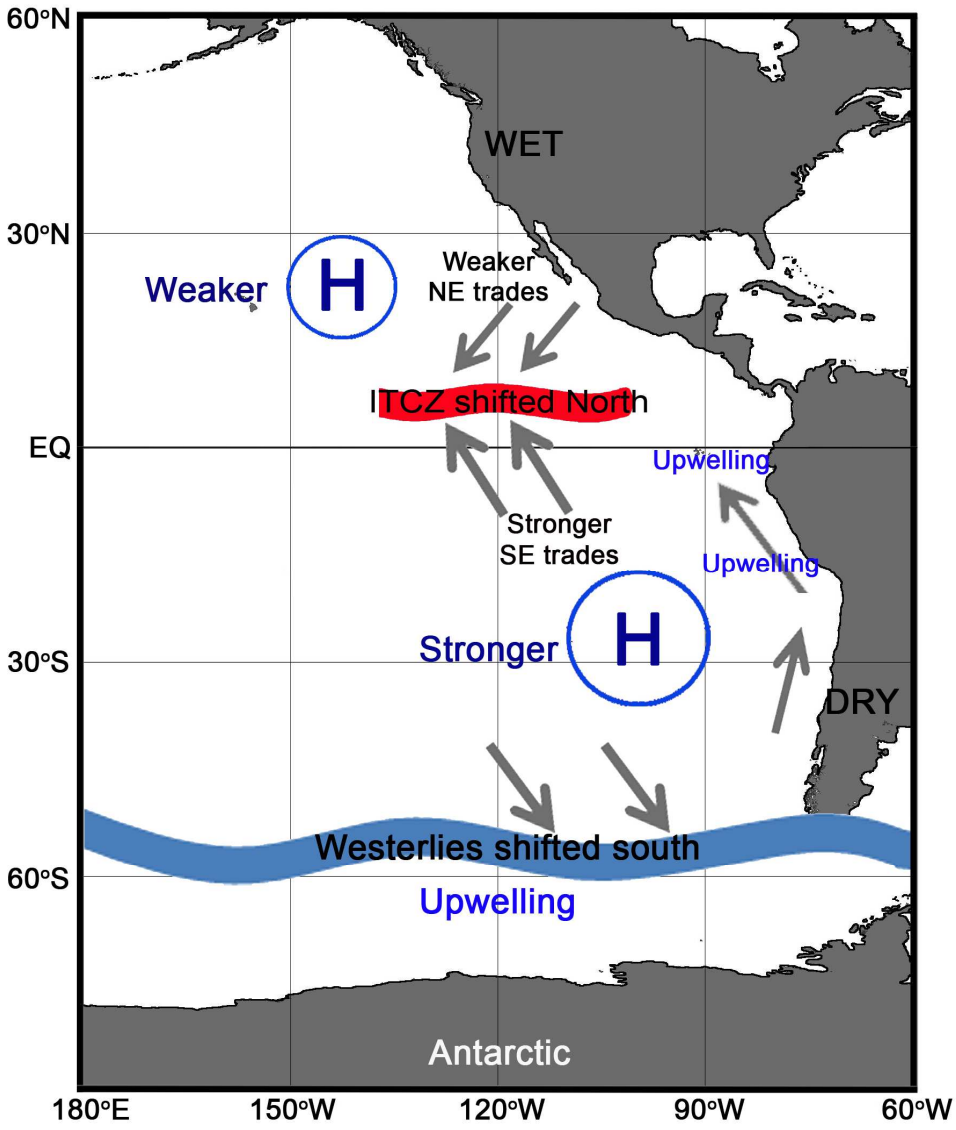

Figure 6. Ocean and atmospheric conditions in the eastern Pacific region during deglaciations. The weaker North Pacific High and the stronger South Pacific High resulted in the northward shift of the ITCZ, the southward shift of the southern westerlies and the intensification of upwelling in the EEP, the Peru margin and the Southern Ocean.

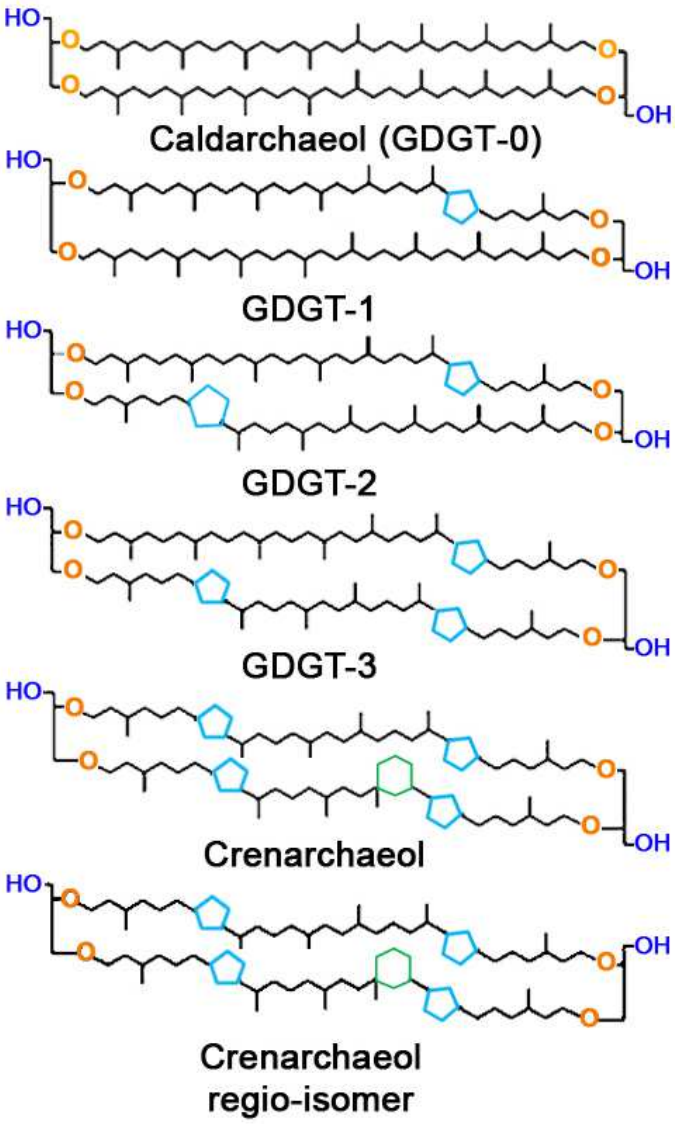

627

628 Appendix I. Structure of glycerol dialkyl glycerol tetraethers

629

630

631

632

633

634